A structural study of Cu–In–Se compounds by x-ray absorption fine structure

Seiji Yamazoe,[a] Hou Kou, and Takahiro Wada
Department of Materials Chemistry, Ryukoku University, Seta, Otsu 520-2194, Japan

(Received 23 September 2010; accepted 16 February 2011)

The local structures about Cu, In, and Se atoms in a series of Cu_2Se–In_2Se_3 pseudobinary compounds have been investigated by x-ray absorption fine structure (XAFS). In K-edge XAFS and L_3-edge x-ray absorption near-edge structure (XANES) suggest that $CuInSe_2$, $Cu_{0.9}InSe_{1.95}$, $Cu_{0.82}InSe_{1.91}$, and $Cu_2In_3Se_{5.5}$ have a nominally four-coordinated $InSe_4$ structure, whereas $CuIn_3Se_5$ and $CuIn_5Se_8$ possess two different $InSe_4$ structures. Cu K-edge XAFS also showed that $CuIn_3Se_5$ and $CuIn_5Se_8$ possess two different $CuSe_4$ structures, whereas others have a $CuSe_4$ structure. Se K-edge XANES and curve fitting analysis reveal that the Cu vacancy (V_{Cu}) gradually forms with decreasing Cu/In ratio. Moreover, the substitution of In for V_{Cu} (In_{Cu}) is observed in $CuIn_3Se_5$ and $CuIn_5Se_8$. These results were compared to the previously proposed Cu–In–Se models. We conclude that $Cu_{0.9}InSe_{1.95}$ and $Cu_{0.82}InSe_{1.91}$ have a chalcopyrite structure with V_{Cu} and that the structure of $CuIn_3Se_5$ and $CuIn_5Se_8$ is a stannite-like structure with V_{Cu} and In_{Cu} defects.

I. INTRODUCTION

$CuInSe_2$ (CIS) and related compounds have attracted much attention as photovoltaic devices because of their strong light absorption and appropriate band gap for absorbing solar radiation.[1,2] An advantage of solar cells made from polycrystalline thin films is that the thickness of the CIS absorption layer is one-hundredth that of crystalline silicon solar cells.[3–5] Efficiencies of 19.9 and 13.5% have been reported for small-scale and large-scale CIS-based solar cells, respectively.[6,7] The CIS absorber usually exhibits p-type conductivity because of the formation of a Cu-poor CIS thin film.[8] In addition, a thin layer of n-type $CuIn_3Se_5$ exists on the surface of a Cu-poor CIS-based absorber. Schmid et al.[8] first reported that the p-type conductivity of the CIS absorber layer and the p-n junction between the p-type CIS and n-type $CuIn_3Se_5$ play important roles in enabling high-efficiency CIS solar cells. A number of structural studies on Cu-poor CIS compounds have been carried out in the last few decades.[9–18] However, the structural details of Cu-poor CIS compounds are still under discussion.

Several phases have been identified in the Cu_2Se–In_2Se_3 pseudobinary system.[10,19] CIS (Cu/In = 1.0) assumes a chalcopyrite structure (α phase). The chalcopyrite structure, which is close to the zincblende structure, has a tetragonal unit cell with space group $I\bar{4}2d$. A key feature of chalcopyrite CIS is that both Cu and In atoms are surrounded by four Se atoms, and the Se atom is coordinated with two Cu and two In atoms. The α phase extends to the composition of $Cu_{0.82}InSe_{1.91}$ (Cu/In = 0.82) in the Cu-poor region. Numerous efforts have been made in structural studies of the Cu-poor α phase to investigate the relationship between electrical properties and defects.[20–23] The chalcopyrite CIS can have variety of defects, such as vacancies, interstitials, and defect pairs. These native defects contribute to the p-type conductivity in CIS. Over the past decade, density functional calculations have shown that the formation energy for the Cu vacancy (V_{Cu}) is small in comparison with other types of vacancies.[24–26] The p-type conductivity of the Cu-poor α phase is thus assumed to be due to the formation of acceptor levels from V_{Cu}. However, no reliable identification of the defect structure has been obtained experimentally and a systematic structural analysis for Cu-poor CIS compounds at the α phase is needed.

In the Cu_2Se–In_2Se_3 pseudobinary system, the β phase extends from the composition of $CuIn_2Se_{3.5}$ (Cu/In = 0.50) to near $CuIn_5Se_8$ (Cu/In = 0.20). For the $CuIn_5Se_8$ (Cu/In = 0.20) phase, two different crystal structures have been reported.[27] The first is the β phase consisting of tetragonal $CuIn_3Se_5$. The other is the γ phase with a hexagonal-layered structure. The β phase structure is similar to the chalcopyrite structure. Since this structure contains many defects, it is difficult to determine the actual structure. Hönle et al.[10] reported that $CuIn_3Se_5$ in the β phase has a space group of $P\bar{4}2c$. This model is supported by Merino et al.[16] because the interatomic distances obtained by x-ray Rietveld analysis resemble realistic values. However, electron diffraction analysis shows that the space group of $CuIn_3Se_5$ is $I\bar{4}2m$, as reported by Hanada et al.[15] They also proposed that an

[a]Address all correspondence to this author.
e-mail: yamazoe@rins.ryukoku.ac.jp
DOI: 10.1557/jmr.2011.63

 © Materials Research Society 2011

https://doi.org/10.1557/jmr.2011.63 Published online by Cambridge University Press

appropriate structural model for $CuIn_3Se_5$ is a stannite-like structure with V_{Cu} and In vacancies (V_{In}). Recently, Paszkowicz et al.[18] proposed another model for $CuIn_3Se_5$ with a space group of $I4(-)2m$ from the Rietveld refinement of x-ray diffraction (XRD) data. These structural models were obtained using only Rietveld refinement of XRD data, and so further studies using other analytical methods are necessary to verify the validity of the models.

X-ray absorption fine structure (XAFS) is a powerful method to investigate the local structure surrounding the absorbing atom, including the valence state. X-ray absorption near-edge structure (XANES) provides information on the electric structure and the structural symmetry surrounding the absorbing atom. Extended x-ray absorption fine structure (EXAFS) also gives information on the local structure of the absorbing atoms; in particular, the coordination number (CN) and bond distance between the absorbing atom and neighboring atoms can be estimated by curve fitting analysis of the EXAFS. Some XAFS studies on Cu-poor CIS compounds have been reported to analyze the defect structure.[17, 28–30] Most studies have focused on the structure of the $CuIn_3Se_5$ (β phase), and so studies on the structure of the Cu-poor α phase are limited. In addition, structural studies on $CuIn_3Se_5$ have been generally conducted using only EXAFS, without a concurrent XANES analysis. Lewandowska et al.[31] reported EXAFS study of Cu–In–Se system. However, they did not analyze the In K-edge XAFS. Merino et al. reported the relationship between the bond length of Cu–Se and In–Se and the Cu/In ratio. However, they did not analyze the Se K-edge XAFS. Chang et al.[17] analyzed Cu K-, In K-, and Se K-edges and obtained a self-consistent set of local structural parameters. However, some of the parameters, such as Debye–Waller factors, were fixed for their analysis of Se K-edge data. Debye–Waller factors influence the CNs and bond lengths. Therefore, it is necessary to fit the CNs and the bond lengths of both Cu–Se and In–Se without fixing Debye–Waller factors. Furthermore, XANES studies were not performed. Bacewicz et al. and Wolska et al. studied Se K-edge XANES for the Cu-poor CIS compounds and proposed that the Cu defects were formed by a decrease in the Cu/In ratio.[28,29] However, they did not analyze the local structures of the other atoms (Cu and In).

In this study, we recorded the Cu K-, In K-, In L_3- and Se K-edges' XAFS spectra of Cu-poor CIS compounds (α phase: $CuInSe_2$, $Cu_{0.9}InSe_{1.95}$, and $Cu_{0.82}InSe_{1.91}$; a mixture of α phase and β phase: $Cu_2In_3Se_{5.5}$; and β phase: $CuIn_3Se_5$ and $CuIn_5Se_8$) and analyzed the local structures of these compounds. From the XANES spectra, the local structures surrounding each atom were estimated by comparison with reference samples with known structures. EXAFS analyses were performed using models consistent with the XANES analyses to obtain structural parameters such as the CN and bond length. Finally, we determined the defect structures of both the α and the β phases by comparison of the obtained structural parameters with some defect models of CIS.

II. EXPERIMENTAL

A. Preparation of CIS and reference samples

Cu–In–Se compounds were prepared by mechanochemical and sintering processes. Six different Cu_2Se–In_2Se_3 pseudobinary compositions ($CuInSe_2$, $Cu_{0.9}InSe_{1.95}$, $Cu_{0.82}InSe_{1.91}$, $Cu_2In_3Se_{5.5}$, $CuIn_3Se_5$, and $CuIn_5Se_8$) were synthesized from elemental powders of Cu, In, and Se.[32] The elemental powders were mixed according to objective molar ratios. The weighed powders were mixed by a planetary ball mill (Fritsch P-7) in a N_2 atmosphere. The ball mill performed the mixing at a speed of 500 rpm for 20 min. The CIS compounds were obtained by heating the mixed powder at 500 °C for 30 min in a N_2 atmosphere. Reference samples such as $ZnIn_2Se_2$, In_2Se_3, $GeSe_2$, and Ga_2Se_3 were also synthesized by the aforementioned method. The phases of the synthesized samples were analyzed by powder XRD.

B. X-ray absorption spectroscopy

X-ray absorption spectra at the Cu K-, In K-, and Se K-edges were taken at the BL01B1 beamline at the SPring-8 facility of the Japan Synchrotron Radiation Research Institute (proposal no. 2010A1197). An Si(111) two-crystal monochromator was used for the incident beam for the Cu K-edge XAFS measurements. The Se K and In K edges' XAFS spectra were recorded using a Si (311) setting for the two-crystal monochromator. The Se K-edge EXAFS spectra for the reference samples were taken at beamline BL-9A in Photon Factory (proposal no. 2009G132). An Si(111) two-crystal monochromator was used. All spectra were recorded in transmission mode, and ion chambers were used for the I_0 and I detectors. The samples, diluted in boron nitride (BN), were placed between the ion chambers. Energy calibration was carried out using a Cu foil for the Cu K-edge and Se K-edge measurements and an In foil for the In K-edge measurement. In L_3-edge, XANES spectra were taken using total electron yield with an Si(220) two-crystal monochromator setting at the BL-10 beamline in the SR center of Ritsumeikan University (proposal no. S21-11). The Cu K-, In K-, and Se K-edges' XAFS spectra, except for the Se K-edge EXAFS spectra of the reference samples, were recorded in the quick scan mode. The Se K-edge EXAFS of the reference samples and In L_3-edge XANES were recorded in step scan mode. Data reduction was carried out using the program REX2000 Ver.2.5.9 (Rigaku Co.). The EXAFS analysis was performed as described later. The χ spectra were extracted by removing the atomic absorption background using a cubic spline and were normalized to

https://doi.org/10.1557/jmr.2011.63 Published online by Cambridge University Press

the edge height. The k^3-weighted χ spectra (χ spectra) were Fourier transformed (FT) into r space, using the Fourier transformation range 3.0–15 $Å^{-1}$. Curve fitting analysis was performed for the first shell (Cu–Se for the Cu K-edge, In–Se for the In K-edge, and Se–M (Cu or In) for the Se K-edge). The passive electron factor (S_0^2) of 1 was used in this study in the curve fitting analysis. The phase and amplitude functions were extracted from CIS, which has a chalcopyrite structure ($I4(-)2d$) by calculation using FEFF8.[33]

III. RESULTS

A. Powder XRD

Figure 1(A) shows XRD patterns for a series of Cu-poor CIS compounds together with the simulated XRD patterns for $CuInSe_2$ [Inorganic Crystal Structure Database (ICSD) no. 70051, $I4(-)2d$] and $CuIn_3Se_5$ ($I4(-)2m$, Ref. 18). The CIS phase exhibited an XRD pattern consistent with the chalcopyrite structure (space group: $I4(-)2d$). Similar XRD patterns were obtained for $Cu_{0.9}InSe_{1.95}$ and $Cu_{0.82}InSe_{1.91}$. In the Cu_2Se–In_2Se_3 system, the structure of Cu-poor CIS compounds with Cu/In ratios from 1.00 to 0.82 was found to be the chalcopyrite α phase with space group $I4(-)2d$. The structures of the $Cu_{0.9}InSe_{1.95}$ and $Cu_{0.82}InSe_{1.91}$ samples synthesized in this study corresponded to those reported in the literature. It has been reported that the lattice constants decrease with decreasing Cu/In ratio.[19] The change in lattice constant with decreasing Cu/In ratio was negligible. Therefore, no distinct diffraction peak shift could be observed in this study.

The XRD patterns of the $Cu_2In_3Se_{5.5}$, $CuIn_3Se_5$, and $CuIn_5Se_8$ samples [Fig. 1(A)] were similar to those of $CuInSe_2$, $Cu_{0.9}InSe_{1.95}$, and $Cu_{0.82}InSe_{1.91}$ and were consistent with the chalcopyrite structure. Extended XRD patterns [Fig. 1(B)], however, showed that the $Cu_2In_3Se_{5.5}$, $CuIn_3Se_5$, and $CuIn_5Se_8$ samples had new diffraction peaks at 21.8°, 34.7°, and 38.0°, respectively. It has been reported that the XRD pattern of the $CuIn_3Se_5$ (β phase) has these diffraction peaks. The space group of $CuIn_3Se_5$ is $I4(-)2m$ as determined by an electron diffraction.[15] In the case of $Cu_2In_3Se_{5.5}$, the diffraction peak at 31.7° attributed to the α phase remained. Therefore, $Cu_2In_3Se_{5.5}$ can be thought of as a mixture of the α phase with space group $I4(-)2d$ and the β phase with space group $I4(-)2m$. The $CuIn_3Se_5$ and $CuIn_5Se_8$ samples are found to be β phase because the characteristic diffraction peak of the α phase at 31.7° was absent. Moreover, the diffraction peak positions in the $CuIn_3Se_5$ and $CuIn_5Se_8$ samples gradually shifted to higher angles with decreasing Cu/In ratio. This shift is attributed to a contraction of the lattice constants. This lattice contraction would seem to be related to the formation of defects in the structure. However, no information on structural defects is provided from the XRD patterns shown in Fig. 1.

B. Cu K-edge XANES

Figure 2 shows the Cu K-edge XANES spectra of several Cu-poor CIS compounds. All samples had the same absorption edge energy, and no pre-edge peak in the range of 8975–8980 eV characterized by the $1s \rightarrow 3d$ forbidden transition of Cu^{2+} species was observed.[34–36]

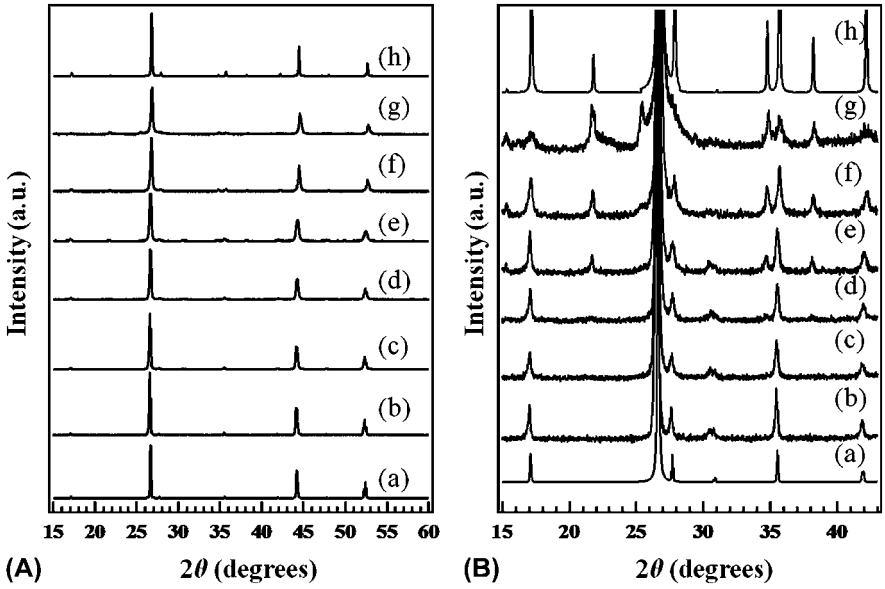


FIG. 1. (A) X-ray diffraction (XRD) patterns of (a) simulation of $CuInSe_2$ [Inorganic Crystal Structure Database (ICSD no. 70051)], (b) $CuInSe_2$, (c) $Cu_{0.9}InSe_{1.95}$, (d) $Cu_{0.82}InSe_{1.91}$, (e) $Cu_2In_3Se_{5.5}$, (f) $CuIn_3Se_5$, (g) $CuIn_5Se_8$, and (h) simulated pattern of $CuIn_3Se_5$ (Ref. 18). (B) Expanded XRD patterns of (a) simulated $CuInSe_2$ (ICSD no. 70051), (b) $CuInSe_2$, (c) $Cu_{0.9}InSe_{1.95}$, (d) $Cu_{0.82}InSe_{1.91}$, (e) $Cu_2In_3Se_{5.5}$, (f) $CuIn_3Se_5$, (g) $CuIn_5Se_8$, and (h) simulated $CuIn_3Se_5$ (Ref. 18).

https://doi.org/10.1557/jmr.2011.63 Published online by Cambridge University Press

Since the only oxidation state of Cu is Cu^+ in CIS, the valence of the Cu atoms in Cu-poor CIS compounds is monovalent and does not affect the Cu/In ratio. The XANES spectra of $Cu_{0.9}InSe_{1.95}$, $Cu_{0.82}InSe_{1.91}$, and $Cu_2In_3Se_{5.5}$ corresponded to that of CIS. Therefore, not only the oxidation state but also the local structure of the Cu atom in $Cu_{0.9}InSe_{1.95}$, $Cu_{0.82}InSe_{1.91}$, and $Cu_2In_3Se_{5.5}$ resemble that of $CuInSe_2$. Although the XANES spectra of $CuIn_3Se_5$ and $CuIn_5Se_8$ were also similar to that of $CuInSe_2$, the intensity of the absorption band appearing at 8992 eV was observed to slightly decrease with decreasing Cu/In ratio. In the Cu oxides, the bands appearing in the XANES region derive from the $1s \rightarrow 4p$ electron transition and the energy positions and the intensities of the bands are sensitive to the local structure of the Cu species.[34,36] Therefore, the decrease in the band intensity observed at 8992 eV in $CuIn_3Se_5$ and $CuIn_5Se_8$ is due to a change in the local structure about the Cu atom relative to that in $CuInSe_2$. It is clear from the XRD patterns shown in Fig. 1 that the $CuIn_3Se_5$ and $CuIn_5Se_8$ samples have a crystal structure different from $CuInSe_2$, $Cu_{0.9}InSe_{1.95}$, and $Cu_{0.82}InSe_{1.91}$. The local structure of Cu atoms in $CuInSe_2$, $Cu_{0.9}InSe_{1.95}$, and $Cu_{0.82}InSe_{1.91}$, for which XRD shown were consistent with the space group of $I4(-)2d$, does not change with decreasing Cu/In ratio. Structural changes around Cu were observed for the $CuIn_3Se_5$ and $CuIn_5Se_8$ samples for which XRD demonstrated a space group of $I4(-)2m$. Therefore, the Cu/In ratio affects the local structure of Cu atom in Cu-poor samples.

C. Cu K-edge EXAFS

The Cu K-edge χ spectra of several Cu-poor CIS compounds are shown in Fig. 3. The χ spectra of $Cu_{0.9}InSe_{1.95}$, $Cu_{0.82}InSe_{1.91}$, and $Cu_2In_3Se_{5.5}$ were similar to those of $CuInSe_2$. On the other hand, a relative decrease in the amplitude of the χ spectra of $CuIn_3Se_5$ and $CuIn_5Se_8$ could be observed with decreasing Cu/In ratio. In addition, the χ spectra range of 3–5 $Å^{-1}$ for $CuIn_3Se_5$ and $CuIn_5Se_8$ were slightly different from those of the other samples. Therefore, it is assumed that a difference in the structural environment around the Cu atom exists between chalcopyrite-type $CuInSe_2$, $Cu_{0.9}InSe_{1.95}$, $Cu_{0.82}InSe_{1.91}$, and $Cu_2In_3Se_{5.5}$, and the others. This result corresponds to that obtained from the Cu K-edge XANES.

Figure 4 shows the FT spectra of the χ spectra shown in Fig. 3. The peak appearing at ~2.0 Å in all spectra is attributed to the Cu–Se bonds. Although the peak intensity of $CuIn_3Se_5$ and $CuIn_5Se_8$ at ~2.0 Å was slightly smaller than that of other compounds ($CuInSe_2$, $Cu_{0.9}InSe_{1.95}$, $Cu_{0.82}InSe_{1.91}$, and $Cu_2In_3Se_{5.5}$), we could not find any remarkable difference among the FT spectra of the samples. We performed fitting analysis against the peak at 1.6–2.4 Å in Fig. 4, which is attributed to the Cu–Se bonds, to obtain the structural parameters of the Cu–Se coordination shells. The structural parameters of the Cu–Se coordination shells are shown in Table I. All samples could be fitted with one unique Cu–Se coordination shell. The CIS sample, which assumes the chalcopyrite structure, showed four Cu–Se bonds with a bond length of 2.413 Å. The average local structure of the Cu atom in CIS as determined by XRD is that Cu has tetrahedral $CuSe_4$ structure with a Cu–Se bond length of 2.414–2.436 Å.[12,21,37–40] The structural parameters determined by EXAFS are in good agreement with those determined by XRD. The CN of all samples is ~4. The bond length of

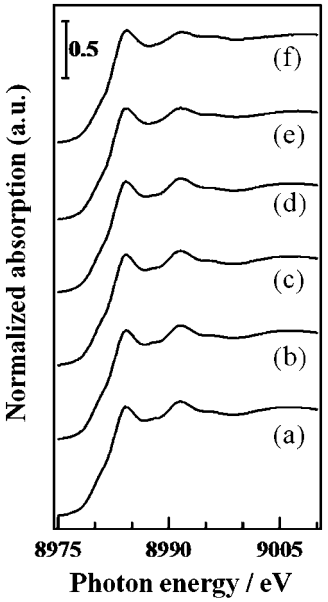


FIG. 2. Cu K-edge x-ray absorption near-edge structure (XANES) spectra of (a) $CuInSe_2$, (b) $Cu_{0.9}InSe_{1.95}$, (c) $Cu_{0.82}InSe_{1.91}$, (d) $Cu_2In_3Se_{5.5}$, (e) $CuIn_3Se_5$, and (f) $CuIn_5Se_8$.

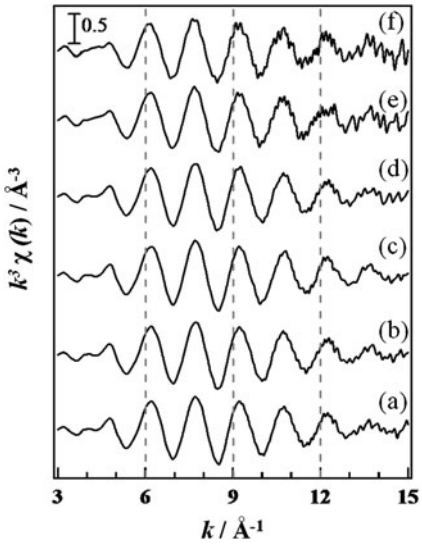


FIG. 3. Cu K-edge χ spectra of (a) $CuInSe_2$, (b) $Cu_{0.9}InSe_{1.95}$, (c) $Cu_{0.82}InSe_{1.91}$, (d) $Cu_2In_3Se_{5.5}$, (e) $CuIn_3Se_5$, and (f) $CuIn_5Se_8$.

https://doi.org/10.1557/jmr.2011.63 Published online by Cambridge University Press

Cu–Se bonds was nearly constant in all samples. The decrease in the amplitude of the χ spectra in the $CuIn_3Se_5$ and $CuIn_5Se_8$ samples, however, cannot be explained by the bond length. Moreover, the *R* factor [*R* factor = $(\Sigma(\chi^{data} - \chi^{fit})^2/\Sigma(\chi^{data})^2)^{1/2}$, here χ^{data} is measured χ data and χ^{fit} is fitted χ function] of the $CuIn_5Se_8$ sample (15%) was slightly high. Therefore, the fitting analysis for the peak in the FT spectra corresponding to the Cu–Se bonds of $CuIn_3Se_5$ and $CuIn_5Se_8$ in Fig. 4 was conducted using two Cu–Se coordination shells. The results are shown in Table I. We can fit them with low *R* factors. Both samples have a shorter Cu–Se bond with a CN of ~1.3 and a longer bond with a CN of ~2.7, and thus the total CN of Cu–Se is 4. If Cu–Se bonds with different bond lengths exist, the amplitude of the EXAFS oscillation will be reduced. In addition, the Cu K-edge XANES spectra of the $CuIn_3Se_5$ and $CuIn_5Se_8$ samples were different from those of the $CuInSe_2$, $Cu_{0.9}InSe_{1.95}$, $Cu_{0.82}InSe_{1.91}$, and $Cu_2In_3Se_{5.5}$ samples. These differences can be explained by the formation of a different Cu–Se bond length in the $CuIn_3Se_5$ and $CuIn_5Se_8$ samples; therefore, we proposed that these samples have four-coordinated $CuSe_4$ species with two different Cu–Se bond lengths.

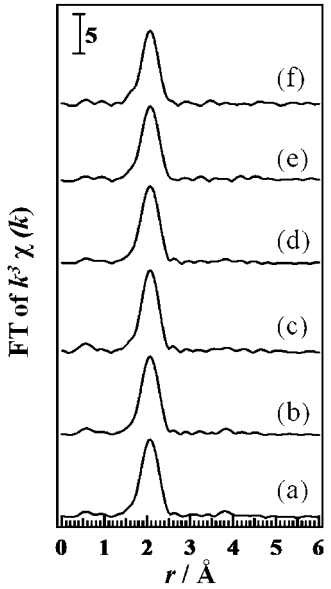


FIG. 4. Fourier transformed (FT) spectra of Cu K-edge χ spectra of (a) $CuInSe_2$, (b) $Cu_{0.9}InSe_{1.95}$, (c) $Cu_{0.82}InSe_{1.91}$, (d) $Cu_2In_3Se_{5.5}$, (e) $CuIn_3Se_5$, and (f) $CuIn_5Se_8$.

TABLE I. Curve fitting results for the Cu–Se shells of Cu-poor Cu–In–Se compounds.

Sample	Cu–Se shell no.	Coordination number	*r* (Å)[a]	$\Delta\sigma^2$ (Å^2)[b]	*R* (%)[c]
$CuInSe_2$	1	3.8 (4)	2.413 (2)	0.0076 (12)	12.2
$Cu_{0.9}InSe_{1.95}$	1	3.8 (4)	2.413 (2)	0.0074 (12)	12.7
$Cu_{0.82}InSe_{1.91}$	1	3.7 (4)	2.413 (2)	0.0071 (12)	12.3
$Cu_2In_3Se_{5.5}$	1	3.9 (4)	2.414 (2)	0.0079 (13)	12.0
$CuIn_3Se_5$	1	3.8 (4)	2.420 (2)	0.0079 (13)	11.5
	2	2.7 (2)	2.448 (15)	0.0001 (18)	0.3
		1.4 (4)	2.362 (16)	0.0001 (19)	
$CuIn_5Se_8$	1	3.6 (3)	2.424 (2)	0.0074 (12)	15.0
	2	2.7 (4)	2.452 (30)	0.0006 (46)	3.2
		1.3 (8)	2.386 (14)	0.0001 (18)	

R fitting range is 1.6–2.5 Å and *k* fitting range is 3.0–15 Å^{-1}.
[a]Bond distance.
[b]Relative Debye–Waller: $\Delta\sigma^2 = (\sigma_{sample} - \sigma_{reference})^2$.
[c]*R* factor: $(\Sigma(\chi^{data} - \chi^{fit})^2/\Sigma(\chi^{data})^2)^{1/2}$.

D. In K-edge and In L_3-edge XANES

Figure 5 shows In K-edge XANES spectra for the samples. All samples exhibited similar XANES spectra, and the In K-edge XANES gave no information on the structural difference in the local structure about the In atom in Cu-poor CIS compounds. On the other hand, the In L_3-edge XANES yielded more structural information on the Cu-poor CIS compounds. Figure 6 shows the In L_3-edge XANES spectra of the various CIS samples. The CIS XANES spectrum is composed of two shoulders and a peak labeled s_1, s_2, and p_1, respectively. A broadening in the s_1 and s_2 peaks and a reduction of p_1 could be observed with decreasing Cu/In ratio in comparing $CuInSe_2$ with $Cu_{0.9}InSe_{1.95}$. The s_1, s_2, and p_1 peaks are attributed to the electron transition from the 2*p* orbital to vacant *s*- or *d*-like orbitals of the absorbing In atom, and their shape and intensity depend on the local structure about the In atoms.[41] Therefore, a decrease in the Cu/In ratio from 1.0 to 0.9 influences the local structure about In atom. The features, s_1, s_2, and p_1, did not significantly change in the $Cu_{0.9}InSe_{1.95}$, $Cu_{0.82}InSe_{1.91}$, and $Cu_2In_3Se_{5.5}$ samples. This result indicates that the local structure around the In atom does not change for Cu/In ratios between 0.9 and 0.67(2/3). Further reduction in the Cu/In ratio (below 2/3) results in broadening of s_1 and s_2 and a gradual decrease in p_1. The drastic change of the In L_3-edge XANES spectra from $Cu_2In_3Se_{5.5}$ to $CuIn_5Se_8$ obviously signifies a structural change around the In atoms. The In L_3-edge spectrum of a $ZnIn_2Se_4$ reference sample is also shown in Fig. 6. There have been two reports about the $ZnIn_2Se_4$ structure reporting that it has a defective stannite structure.[42,43] The first report stated that $ZnIn_2Se_4$ has three kinds of In sites and the other report stated that $ZnIn_2Se_4$ has two types of In sites. All In atoms in both structures are tetrahedrally coordinated by Se, e.g., $InSe_4$. The differences between the different $InSe_4$ environments lie in the Se–In–Se angle. The XANES spectrum of $ZnIn_2Se_4$ resembles that of $CuIn_5Se_8$. Therefore, it is expected that some $InSe_4$ species with different Se–In–Se angle exist in $CuIn_5Se_8$, according to $ZnIn_2Se_4$.

https://doi.org/10.1557/jmr.2011.63 Published online by Cambridge University Press

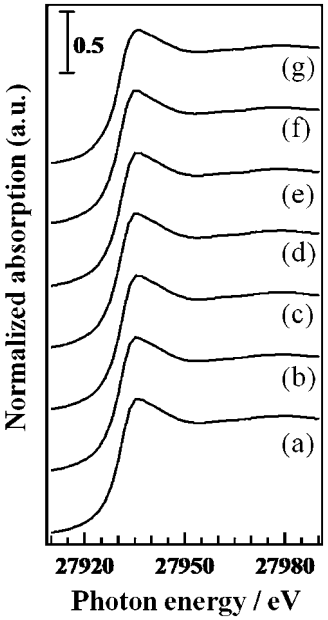


FIG. 5. In K-edge XANES spectra of (a) $CuInSe_2$, (b) $Cu_{0.9}InSe_{1.95}$, (c) $Cu_{0.82}InSe_{1.91}$, (d) $Cu_2In_3Se_{5.5}$, (e) $CuIn_3Se_5$, (f) $CuIn_5Se_8$, and (g) $ZnIn_2Se_4$.

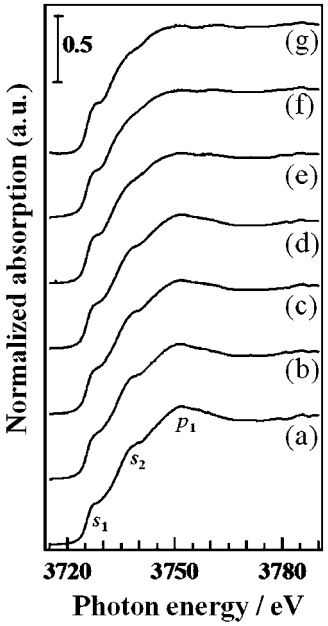


FIG. 6. In L_3-edge XANES spectra of (a) $CuInSe_2$, (b) $Cu_{0.9}InSe_{1.95}$, (c) $Cu_{0.82}InSe_{1.91}$, (d) $Cu_2In_3Se_{5.5}$, (e) $CuIn_3Se_5$, (f) $CuIn_5Se_8$, and (g) $ZnIn_2Se_4$.

E. In K-edge EXAFS

Figure 7 shows the In K-edge χ spectra of the samples. The oscillation patterns of the Cu-poor CIS samples are similar to that of CIS. Although the amplitude of the oscillations in the $CuInSe_2$, $Cu_{0.9}InSe_{1.95}$, $Cu_{0.82}InSe_{1.91}$, and $Cu_2In_3Se_{5.5}$ samples was almost the same, as that in $CuIn_3Se_5$ and $CuIn_5Se_8$, the amplitude was observed to gradually decrease with decreasing Cu/In ratio. The reduction in the amplitude can be clearly seen in the FT spectra, as shown in Fig. 8. The peak appearing at 2.0–2.3 Å is attributed to the In–Se bonds. The peak intensities of $CuIn_3Se_5$ and, especially, $CuIn_5Se_8$ were smaller to those of the other samples, $CuInSe_2$, $Cu_{0.9}InSe_{1.95}$, $Cu_{0.82}InSe_{1.91}$, and $Cu_2In_3Se_{5.5}$. The reductions in the amplitude of the χ spectra and the peak intensity of the FT spectra in $CuIn_3Se_5$ and $CuIn_5Se_8$ samples are due to the change in the local structure of the In atom. The main causes for these reductions are the decrease in the CN around In atom and the formation of the In species with different local structure. In light of the results of the In L_3-edge XANES spectra, the presence of structurally different $InSe_4$ coordination is more likely in $CuIn_3Se_5$ and $CuIn_5Se_8$ samples. We have fit the FT from 2.0 to 2.3 Å as shown in Fig. 8 to obtain the structural information about In–Se bonds. The structural parameters of the In–Se coordination shell are shown in Table II. The $CuInSe_2$, $Cu_{0.9}InSe_{1.95}$, $Cu_{0.82}InSe_{1.91}$, and $Cu_2In_3Se_{5.5}$ samples can be fit using a single In–Se coordination shell. Chalcopyrite CIS showed the four In–Se bonds with a bond length of 2.584 Å. It has been reported from XRD analyses that the local structure about an In atom in CIS can be characterized by $InSe_4$ tetrahedral building blocks with a In–Se bond length of 2.558–2.602 Å.[12,21,37–40] The structural parameters obtained in this study are in good agreement with values reported in the literature. The CN and the bond length of the In–Se bonds in the $Cu_{0.9}InSe_{1.95}$, $Cu_{0.82}InSe_{1.91}$, and $Cu_2In_3Se_{5.5}$ samples nearly match those of $CuInSe_2$. This result corresponds to the result of In L_3-edge XANES spectra. The $CuIn_3Se_5$ and $CuIn_5Se_8$ samples can be fitted with one In–Se shell. However, the CN of In–Se shell was close to 3 and the *R* factor became larger than in other samples. In the In L_3-edge XANES, we demonstrated that the local structure of the $CuIn_5Se_8$ resembles that of the $ZnIn_2Se_4$. The $ZnIn_2Se_4$ has some four-coordinated $InSe_4$ structures. Thus, we carried out the fitting analysis using two In–Se coordination shells for the $CuIn_3Se_5$ and $CuIn_5Se_8$ samples. Obtained data are shown in Table II. Although the CN of the shorter In–Se shell is smaller than that of the longer one in both samples, the total CN is ~4. The In L_3-edge XANES and the In K-edge EXAFS spectra indicate that two kinds of $InSe_4$ coordination polyhedron with different local structures are present in the $CuIn_3Se_5$ and $CuIn_5Se_8$ samples. Therefore, a fitting analysis would indicate that an $[InSe_4]_{long}$ ($[InSe_4]_{long}$: longer In–Se bond) and an $[InSe_4]_{short}$ ($[InSe_4]_{short}$: shorter In–Se bond) coordination polyhedron exist with the abundance ratios ($[InSe_4]_{long}$:$[InSe_4]_{short}$) of 2.3:1.6 and 2.3:1.4 in the $CuIn_3Se_5$ and $CuIn_5Se_8$ samples, respectively. These ratios are important for determining the structure of the Cu-poor CIS compound with space group of $I\bar{4}2m$. A detailed discussion of the structure follows later.

https://doi.org/10.1557/jmr.2011.63 Published online by Cambridge University Press

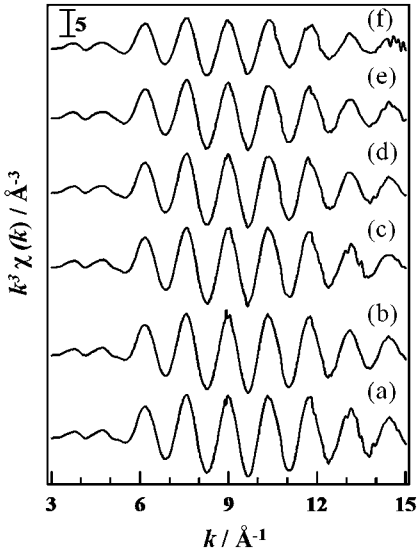


FIG. 7. In K-edge χ spectra of (a) $CuInSe_2$, (b) $Cu_{0.9}InSe_{1.95}$, (c) $Cu_{0.82}InSe_{1.91}$, (d) $Cu_2In_3Se_{5.5}$, (e) $CuIn_3Se_5$, and (f) $CuIn_5Se_8$.

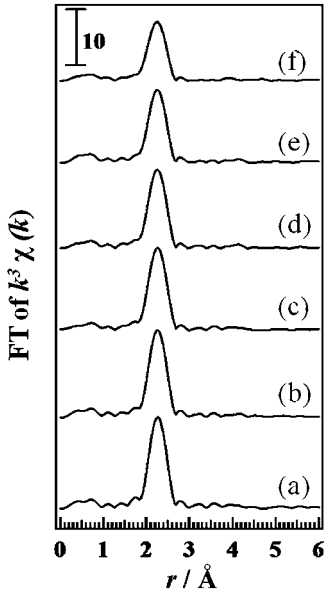


FIG. 8. FT spectra of In K-edge χ spectra of (a) $CuInSe_2$, (b) $Cu_{0.9}InSe_{1.95}$, (c) $Cu_{0.82}InSe_{1.91}$, (d) $Cu_2In_3Se_{5.5}$, (e) $CuIn_3Se_5$, and (f) $CuIn_5Se_8$.

F. Se K-edge XANES

Figure 9(A) shows the Se K-edge XANES spectra of the samples. The CIS sample showed a small post-edge peak at 12,648.2 eV (P_1) and a large and broad post-edge peak at 12,651.8 eV (P_2). Decreasing Cu/In ratio results an increase in the intensity of the P_1 peak and a gradual decrease in the intensity of the P_2 peak with isosbestic points [as shown in Fig. 9(B)] in $CuInSe_2$, $Cu_{0.9}InSe_{1.95}$, $Cu_{0.82}InSe_{1.91}$, $Cu_2In_3Se_{5.5}$, and $CuIn_3Se_5$. This implies that the structural differences around Se occurred with decreasing Cu/In ratio. On the other hand, the XANES spectrum of $CuIn_5Se_8$ is close to that of $CuIn_3Se_5$. Therefore, changes in the local structure about Se for samples with Cu/In ratios between 0.20 and 0.33 are not negligible. Wolska et al. reported that the P_1 and P_2 peaks correspond to the In(s, p)–Se(p) antibonding orbital and the Se p-like density of states hybridized with Cu(s) and In(p) states, respectively.[28,29] These peak intensities depend on the symmetry around the Se atoms. Studies of Se K-edge XANES are limited.

To further understand the Se K-edge XANES, we recorded XANES spectra of some reference compounds ($CuGaSe_2$, In_2Se_3, $GeSe_2$, Ga_2Se_3, and $ZnIn_2Se_4$) whose structures have already been determined. The XANES spectra of the reference compounds are also shown in Fig. 9(A). In the XANES spectrum of $CuGaSe_2$, which has the chalcopyrite structure (space group: $I\bar{4}2d$, ICSD no. 28737), the P_1 peak intensity is as small as that of CIS. This is because the local structure about the Se atom (Se bonds with two Cu atoms and two In atoms in a tetrahedral arrangement) in CIS is close to that in $CuGaSe_2$, in which Se bonds with two Cu and two Ga atoms. On the other hand, the P_1 peak intensities of $ZnIn_2Se_4$ and In_2Se_3 are similar to those of $CuIn_3Se_5$ and $CuIn_5Se_8$. The crystal structures of $ZnIn_2Se_4$ and In_2Se_3, confirmed by XRD measurements, are $I\bar{4}$ (ICSD no. 40798) [or $I\bar{4}m$ (ICSD no 68216)] and $P61$ (ICSD no. 1376), respectively. The local structure around Se in $ZnIn_2Se_4$ is characterized by a nominally threefold coordinated Se atom, whereas In_2Se_3 has two types of threefold coordinated Se sites. Ga_2Se_3 (space group: Cc, ICSD no. 35028) has 2- to 3-fold coordinated Se atoms with a larger P_1 peak intensity than that of In_2Se_3. Moreover, $GeSe_2$ (space group: $P2_1/c$, ICSD no. 614), which has only twofold coordinated Se atoms, showed the largest P_1 peak intensity among all the samples. These results clearly showed that the CN between the Se atom and the neighboring atoms affects the P_1 peak intensity and also showed that the decrease in

TABLE II. Curve fitting results for the In–Se shells of Cu-poor Cu–In–Se compounds.

Sample	In–Se shell no.	CN	r (Å)[a]	$\Delta\sigma^2$ (Å^2)[b]	R (%)[c]
$CuInSe_2$	1	3.9 (4)	2.584 (5)	0.0001 (1)	3.3
$Cu_{0.9}InSe_{1.95}$	1	3.8 (4)	2.583 (5)	0.0001 (1)	5.2
$Cu_{0.82}InSe_{1.91}$	1	4.1 (4)	2.583 (5)	0.0001 (1)	5.3
$Cu_2In_3Se_{5.5}$	1	3.9 (4)	2.580 (5)	0.0001 (1)	4.3
$CuIn_3Se_5$	1	3.4 (4)	2.567 (2)	0.0001 (1)	11.7
	2	2.3 (1.1)	2.642 (39)	0.0006 (82)	0.9
		1.6 (1.1)	2.549 (35)	0.0015 (154)	
$CuIn_5Se_8$	1	3.2 (3)	2.567 (2)	0.0001 (3)	10.8
	2	2.3 (8)	2.645 (32)	0.0004 (36)	1.0
		1.4 (8)	2.550 (29)	0.0014 (120)	

R fitting range is 1.8–2.6 Å and k fitting range is 3.0–15 Å^{-1}.
[a]Bond distance.
[b]Relative Debye–Waller: $\Delta\sigma^2 = (\sigma_{sample} - \sigma_{reference})^2$.
[c]R factor: $(\Sigma(\chi^{data} - \chi^{fit})^2/\Sigma(\chi^{data})^2)^{1/2}$.

https://doi.org/10.1557/jmr.2011.63 Published online by Cambridge University Press

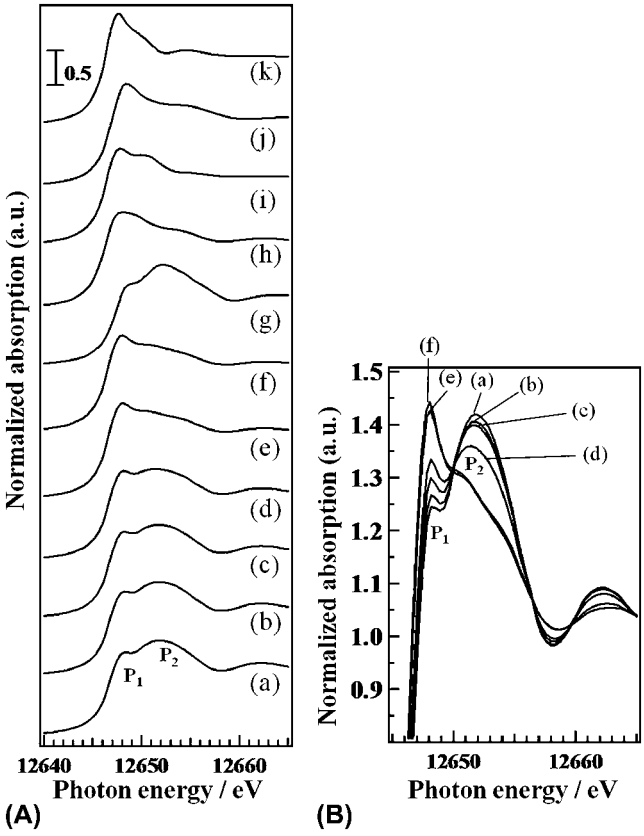


FIG. 9. (A) Se K-edge XANES spectra of (a) $CuInSe_2$, (b) $Cu_{0.9}InSe_{1.95}$, (c) $Cu_{0.82}InSe_{1.91}$, (d) $Cu_2In_3Se_{5.5}$, (e) $CuIn_3Se_5$, (f) $CuIn_5Se_8$, (g) $CuGaSe_2$, (h) $ZnIn_2Se_4$, (i) In_2Se_3, (j) Ga_2Se_3, and (k) $GeSe_2$. (B) Superimposed Se K-edge XANES spectra of (a) $CuInSe_2$, (b) $Cu_{0.9}InSe_{1.95}$, (c) $Cu_{0.82}InSe_{1.91}$, (d) $Cu_2In_3Se_{5.5}$, (e) $CuIn_3Se_5$, and (f) $CuIn_5Se_8$.

the CN of the Se atom leads to an increase in the P_1 peak intensity. Wolska et al.[29] reported that the symmetry of the tetrahedral SeM_4 (M = Cu and In) structure, including the V_{Cu} and the incorporation of the In atom in V_{Cu} (In_{Cu}), influences the P_1 peak intensity and distortions from T_d symmetry and defects, such as V_{Cu} and In_{Cu} in the tetrahedral SeM_4 structure, enlarge the P_1 peak intensity in the Cu–In–Se system including CIS. This relationship between the local structure of Se and the P_1 peak intensity may extend to the other Se compounds as the P_1 intensity of CIS is larger than that of $CuGaSe_2$ whose Se structure is closer to T_d symmetry than that of CIS. Therefore, the relationship between the increase in P_1 intensity to a reduction in the CN of Se obtained in this study agrees with Wolska's results.[29]

In Fig. 9(A), it can be seen that the P_1 intensity of $CuIn_3Se_5$ and $CuIn_5Se_8$ correspond to that of $ZnIn_2Se_4$ and In_2Se_3 with threefold coordinated Se atoms. Therefore, the CN of the Se atoms falls with decreasing Cu/In ratio. This implies the formation of cation vacancies such as V_{Cu}. Moreover, the correspondence of the P_1 peak intensities of $CuIn_3Se_5$ and $CuIn_5Se_8$ to those of $ZnIn_2Se_4$ and In_2Se_3 indicates that the Se atoms in the $CuIn_3Se_5$ and $CuIn_5Se_8$ have threefold coordinated structure. In this way, the P_1 peak intensity is important for analyzing the local structure of Se atom in the metal selenide.

G. Se K-edge EXAFS

Figure 10 shows the Se K-edge χ spectra of a series of Cu_2Se–In_2Se_3 pseudobinary compounds. The Cu-poor CIS samples exhibited a similar oscillation pattern to CIS. However, the amplitude of the oscillations was gradually reduced by decreasing the Cu/In ratio. Considering the results obtained by the Se K-edge XANES spectra, the reduced amplitude is likely due to a decrease in the CN of Se atoms. The FT spectra of the Se K-edge χ spectra are shown in Fig. 11. The peak appearing at 2.0−2.6 Å is attributed to the Se–M (M = Cu and/or In) bond. The peak intensity at 2.0−2.6 Å was gradually reduced with the decrease in the Cu/In ratio, according to the behavior of the amplitude in the Se K-edge χ spectra. A curve fitting analysis of the Se–M peak of the FT spectra was carried out to obtain structural information of the samples. All samples could be fitted with an Se–Cu shell and an Se–In shell. The obtained parameters of the samples are shown in Table III. In the case of $CuIn_3Se_5$ and $CuIn_5Se_8$, the obtained parameters are the average of two Cu–Se bonds and two In–Se bonds. The Se atom in the CIS sample had a four-coordinated structure with two Se–Cu bonds and two Se–In bonds. The bond lengths of the Se–Cu and Se–In bonds were 2.413 and 2.589 Å, respectively. Both bond lengths correspond to those obtained by the fitting analysis of the Cu K-edge EXAFS and the In K-edge EXAFS, as shown in Tables I and II. The chalcopyrite CIS has a tetrahedral Se species surrounded by two Cu and two In atoms. The reported bond lengths of the Se–Cu and Se–In bonds are 2.414−2.436 Å and 2.558−2.602 Å, respectively.[12,21,37–40] The obtained parameters in the fitting analysis are close to the reported values. The bond lengths of Se–Cu and Se–In and the CN of the Se–In shell do not change with decreasing Cu/In ratio. The CN of the Se–Cu shell, however, was found to gradually decrease with decreasing Cu/In ratio. This means that the Cu-poor CIS in the Cu/In range from 1 to 2/3 have V_{Cu} and In_{Cu} concentrations are not detectable. On the other hand, not only do the number of Se–Cu bonds decrease but there is also a corresponding increase in the number of Se–In bonds in $CuIn_3Se_5$ and $CuIn_5Se_8$. The total CN of both samples was ~3. Therefore, the replacement of the In atoms on V_{Cu} sites may occur in $CuIn_3Se_5$ and $CuIn_5Se_8$. The Se K-edge XANES spectra provide information on the local structure around the Se atom. An analysis of the XANES spectra suggests that the CN of Se falls with decreasing Cu/In ratio. The results from a fitting analysis yielded a CN of Se that was in excellent agreement with the results obtained from a XANES

https://doi.org/10.1557/jmr.2011.63 Published online by Cambridge University Press

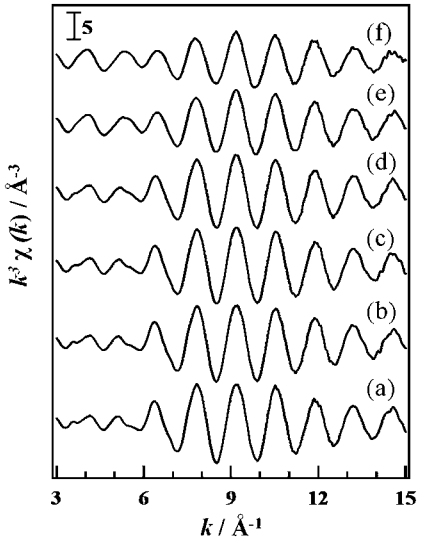


FIG. 10. Se K-edge χ spectra of (a) $CuInSe_2$, (b) $Cu_{0.9}InSe_{1.95}$, (c) $Cu_{0.82}InSe_{1.91}$, (d) $Cu_2In_3Se_{5.5}$, (e) $CuIn_3Se_5$, and (f) $CuIn_5Se_8$.

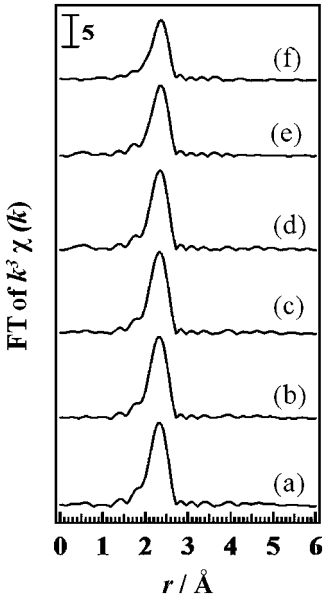


FIG. 11. FT spectra Se K-edge χ spectra of (a) $CuInSe_2$, (b) $Cu_{0.9}InSe_{1.95}$, (c) $Cu_{0.82}InSe_{1.91}$, (d) $Cu_2In_3Se_{5.5}$, (e) $CuIn_3Se_5$, and (f) $CuIn_5Se_8$.

spectra analysis. The bond length behavior of the Se–Cu and Se–In bonds as a function of the Cu/In ratio resulting from a curve fitting analysis of the Se K-edge EXAFS demonstrates the same tendency as that obtained from a fitting analyses of the Cu K-edge and In K-edge EXAFS.

IV. DISCUSSION

A. A structural model for the α phase of $CuInSe_2$, $Cu_{0.9}InSe_{1.95}$, and $Cu_{0.82}InSe_{1.91}$

The $CuInSe_2$, $Cu_{0.9}InSe_{1.95}$, and $Cu_{0.82}InSe_{1.91}$ samples have a chalcopyrite structure ($I\bar{4}2d$), as determined from the XRD pattern shown in Fig. 1. XAFS analysis showed that CIS has four-coordinated $CuSe_4$, $InSe_4$, and SeM_4 (M = 2Cu and 2In) polyhedra. The bond lengths of Cu–Se and In–Se, determined by the Cu K-edge and In K-edge EXAFS analyses, were 2.413 and 2.584 Å, respectively, and these values corresponded to those obtained by an analysis of Se K-edge EXAFS data. Figure 12(a) shows the conventional unit cell for the chalcopyrite structure with space group of $I\bar{4}2d$.[37] The CNs of Cu, In, and Se and the shell lengths of Cu–Se and In–Se, obtained in this study, are in good agreement with reported values.[12,21,37–40] Therefore, the results of the XAFS analyses in this study are reliable. A decrease in the Cu/In ratio from 1 to 0.82 results in a reduction in the CN of the Se–Cu shell for the Se-centered tetrahedron, as obtained by an analysis of Se K-edge data. Other structural parameters, such as the CN of the Cu-centered Cu–Se shells, the In-centered In–Se shells, Se-centered Se–In shells, and all the bond lengths, did not change. These results clearly indicate an increase in V_{Cu} in the chalcopyrite structure with decreasing Cu/In ratio, as shown in Fig. 12(b). It has been reported that V_{Cu} and a complex defect involving In_{Cu} are easily formed in the CIS chalcopyrite structure based on first principle studies of defect formation energies for CIS.[24–26] Since the CN of the Se-centered Se–In shell does not change with decreasing Cu/In ratio, the In_{Cu} complex defect cannot exist in the $Cu_{0.9}InSe_{1.95}$ and $Cu_{0.82}InSe_{1.91}$ samples. The presence of V_{Cu} is in good agreement with the results obtained by first principle studies. Moreover, it is known that the Cu-poor CIS thin film shows p-type conductivity, a fact critical for the efficiency of CIS solar cells.[8] The origin of the p-type conductivity is thought to be due to the formation of V_{Cu}. The formation of a V_{Cu} creates a hole, and this hole acts as

TABLE III. Curve fitting results for the Se–M (M = Cu, In) shells of Cu-poor Cu–In–Se compounds.

Sample	Atom (In–Se shell no.)	CN	R (Å)[a]	$\Delta\sigma^2$ (Å^2)[b]	R (%)[c]
$CuInSe_2$	Cu	1.9 (8)	2.413 (8)	0.0003 (41)	3.4
	In	1.9 (5)	2.589 (9)	0.0001 (7)	
$Cu_{0.9}InSe_2$	Cu	1.8 (8)	2.412 (9)	0.0002 (43)	6.5
	In	1.9 (5)	2.585 (10)	0.0001 (8)	
$Cu_{0.82}InSe_2$	Cu	1.7 (7)	2.412 (10)	0.0002 (42)	4.8
	In	1.9 (5)	2.586 (10)	0.0001 (6)	
$Cu_2In_3Se_{5.5}$	Cu	1.5 (7)	2.412 (11)	0.0002 (56)	5.2
	In	2.0 (5)	2.585 (9)	0.0001 (5)	
$CuIn_3Se_5$	Cu	0.9 (7)	2.419 (22)	0.0003 (134)	2.7
	In	2.2 (5)	2.583 (9)	0.0001 (3)	
$CuIn_5Se_8$	Cu	0.5 (5)	2.424 (30)	0.0002 (142)	5.1
	In	2.4 (4)	2.579 (7)	0.0001 (4)	

R fitting range is 1.8–2.7 Å and k fitting range is 3.0–15 Å^{-1}.
[a]Bond distance.
[b]Relative Debye–Waller: $\Delta\sigma^2 = (\sigma_{sample} - \sigma_{reference})^2$.
[c]R factor: $(\Sigma(\chi^{data} - \chi^{fit})^2/\Sigma(\chi^{data})^2)^{1/2}$.

https://doi.org/10.1557/jmr.2011.63 Published online by Cambridge University Press

a carrier giving rise to p-type conductivity. From the above mentioned results, the structural model of the α phase with a space group of $I4(-)2d$ and the Cu/In ratio ranging from 1 to 0.82 is the chalcopyrite structure with a V_{Cu}, as shown in Fig. 12(b).

B. Structural model of β phase, $CuIn_3Se_5$, and $CuIn_5Se_8$

An analysis of the XRD patterns of $CuIn_3Se_5$ and $CuIn_5Se_8$ demonstrated that they crystallized in the β phase. The β phase has a similar structure to the chalcopyrite structure. Hönle et al.[10] reported that $CuIn_3Se_5$ has the space group $P4(-)2c$, and this model is supported by Merino et al.[16] The Hönle model is shown in Fig. 13(a), and the structural parameters obtained by an XRD analysis are shown in Table IV. This structure has one Cu atom site and three In (In1, In2, and In3) atom sites. The average local structures of Cu, In, and Se are also shown in Table V. The Cu atom has a tetrahedral $CuSe_4$-coordinated environment with a Cu–Se bond length of 2.420 Å. The local structure about In is characterized by a In2–Se bond length equal to that of In3–Se. Therefore, an average tetrahedral $InSe_4$ fragment possesses two kinds of In–Se bonds, namely an In1–Se bond with a length of 2.615 Å with a CN of 1.9 and an In2(3)–Se shell with a length of 2.470 Å and a CN of 2.1. The average local structure of an Se atom has a CN of about 0.7 and 2.3 for Se–Cu (2.420 Å) and Se–In (2.537 Å), respectively. An XAFS analysis of the $CuIn_3Se_5$ sample of the local structure about the Se atom is consistent with that of the Hönle model. However, the local structure about the Cu atom and the CNs of the long (In1–Se) and short (In2(3)–Se) In–Se shells differ from the Hönle model. Moreover, an electron diffraction analysis showed that $CuIn_3Se_5$ has the space group $I4(-)2m$. Therefore, this model is inconsistent with the $CuIn_3Se_5$ structure. There are two high integrity models for the $CuIn_3Se_5$, proposed by Hanada et al.[15] and Paszkowicz et al.[18]

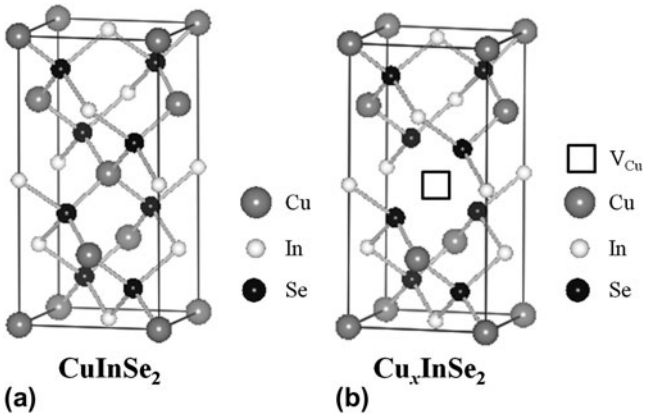


FIG. 12. (a) Structure of chalcopyrite $CuInSe_2$ and (b) proposed crystal structure of Cu-poor Cu–In–Se compounds ($0.82 < Cu/In < 1.0$).

Figure 13(b) shows the Hanada model as refined by Merino, which is a stannite-like structure with V_{Cu} and In vacancies (V_{In}).[15,16] In this model, there is one kind of $CuSe_4$ polyhedron and there are two kinds of $InSe_4$ polyhedron (In1 and In2). Structural parameters such as the lattice constant, crystallographic site, and occupancy are shown in Table IV. The average local structure about Cu, In, and Se atoms using the Hanada model is shown in Table V. The Cu atom bonds to four Se atoms with a bond length of 2.273 Å. The average tetrahedral $InSe_4$ has two kinds of In–Se bonds since the occupancies of the In1 site (4d site) and the In2 (2b site) site are 1 and 0.4, respectively. Therefore, the average structure of the $InSe_4$ fragments in the Hanada model have CNs of 3.3 for In1–Se (bond length = 2.529 Å) and 0.7 for In2–Se (2.676 Å) (average bond length of In–Se is 2.555 Å.). The local structure of the Se atom has CNs and bond lengths of 2.4 and 2.555 Å for Se–In and 0.8 and 2.273 Å for Se–Cu, respectively. Compared with the structural parameters of $CuIn_3Se_5$ obtained from the present XAFS analysis (Table I), the CNs of In–Se shells for the In site are quite different. Although the CNs of the short and long In–Se shells determined by the present XAFS analysis are 1.6 and 2.3, respectively, CNs from the Hanada model are 3.3 and 0.7, respectively. Moreover, the bond length of the Cu–Se bonds determined by the XAFS analysis (2.424 Å) is much larger (>0.1 Å) than that estimated from the Hanada model (2.273 Å). Therefore, the results of the XAFS analysis are inconsistent with the Hanada model.

Paszkowicz et al.[18] proposed another structure model of the $CuIn_3Se_5$ based on the $I4(-)2m$ space group using Rietveld refinement of powder XRD data, as shown in Fig. 13(c). This model is similar to the Hanada model; however, the occupancies of the Cu and In atoms for each site are different. The structural parameters for the Paszkowicz model are shown in Table IV. Two type of Cu sites (Cu1 and Cu2) and two types of In (In1 and In2) sites exist in this model. In the light of the occupancies of the atoms, the average local structure about Cu atom is a four-coordinated $CuSe_4$ polyhedron consisting of Cu1–Se with a CN of 2.7 and a bond length of 2.564 Å and Cu2–Se with a CN of 1.3 and a bond length of 2.304 Å, as shown in Table V. In also has a four-coordinated $InSe_4$ structure. The average $InSe_4$ structure has two different bonds, the first with a coordination number of 2.5 and a bond length of 2.564 Å and a second with coordination number 1.5 and a bond length of 2.565 Å. The average Cu–Se and In–Se bond lengths are 2.480 and 2.564 Å, respectively. The local structure about Se has a Se–Cu coordination number of 0.8 with a bond length of 2.480 Å and a Se–In coordination number of 2.3 with a bond length of 2.564 Å. Compared with the local structures about the Cu, In, and Se atoms in $CuIn_3Se_5$ obtained by an XAFS analysis (Tables I–III), the bond lengths of Cu1–Se and Cu2–Se in the Cu-centered $CuSe_4$ polyhedron and those of

https://doi.org/10.1557/jmr.2011.63 Published online by Cambridge University Press

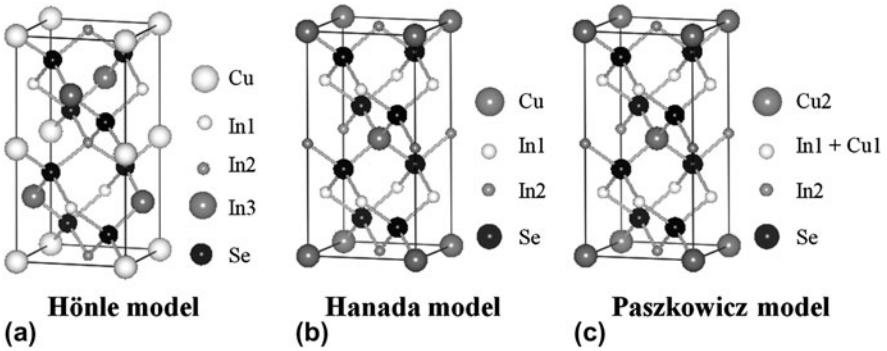


FIG. 13. Crystal structures of (a) Hönle, (b) Hanada, and (c) Paszkowicz models of $CuIn_3Se_5$.

TABLE IV. Structural parameters of different $CuIn_3Se_5$ models.

Model	Space group	Lattice constant (Å)	Atomic construction	
			Site	Occupancy
Hönle et al.[10]; Merino et al.[16]	*P*4(−)2c	*a* 5.755	8n	0.9(Se)
		c 11.52	2d	1.0(In1)
			2b	0.57(In2) (0.02(Cu))
			2e	0.68(Cu)
			2f	0.6(In3) (Cu(0.02))
Hanada et al.[15]; Merino et al.[16]	*I*4(−)2m	*a* 5.754	8i	1.0(Se)
		c 11.518	4d	1.0(In1)
			2b	0.4(In2)
			2a	0.8(Cu)
Paszkowicz et al.[18]	*I*4(−)2m	*a* 5.758	8i	1.0(Se)
		c 11.536	4d	0.73(In1)
				0.27(Cu1)
			2b	0.88(In2)
			2a	0.27(Cu2)

TABLE V. Average structures of $CuSe_4$, $InSe_4$, and SeM_4 (M = Cu, In) fragments in different $CuIn_3Se_5$ models.

Model	$CuSe_4$			$InSe_4$			SeM_4 (M = Cu, In)		
	Bond	CN	*r* (Å)[a]	Bond	CN	*r* (Å)[a]	Bond	CN	*r* (Å)[a]
Hönle et al.[10]; Merino et al.[16]	Cu–Se	4.0	2.420	In1–Se	1.9	2.615	Se–Cu	0.7	2.420
				In2(3)–Se	2.1	2.470	Se–In	2.3	2.537
Hanada et al.[15]; Merino et al.[16]	Cu–Se	4.0	2.273	In1–Se	3.3	2.529	Se–Cu	0.8	2.273
				In2–Se	0.7	2.676	Se–In	2.4	2.555
Paszkowicz et al.[18]	Cu1–Se	2.7	2.564	In1–Se	2.5	2.564	Se–Cu	0.8	2.480
	Cu2–Se	1.3	2.304	In2–Se	1.5	2.565	Se–In	2.3	2.564

[a]Bond distance.

In1–Se and In2–Se in the In-centered $InSe_4$ polyhedron are slightly different (<0.12 Å). However, the coordination numbers of these shells in the Paszkowicz model are in accord with the results of the Cu K-edge and In K-edge XAFS analysis (2.7 for Cu1–Se, 1.4 for Cu2–Se, 1.6 for In1–Se, and 2.3 for In2–Se, in Tables I and II). Moreover, the coordination numbers and the bond lengths of Se centered Se–Cu and Se–In polyhedron mostly correspond to those obtained from a Se K-edge XAFS analysis. The XRD pattern reflects average periodic long-range atomic order. The XRD analysis yields the location of crystallographic sites and their occupancies. The bond lengths are determined by the distance between the crystallographic sites. In contrast, XAFS indicates the average local structure around the target atom. Local structures such as symmetry, bond lengths, and coordination numbers are well determined by the XANES and EXAFS data. However, the XAFS data does not include information on long-range order. The difference in the bond lengths (<0.12 Å) between the XRD analysis in the Paszkowicz model and the XAFS analysis is due to the differences in the measuring methods. On the other hand,

https://doi.org/10.1557/jmr.2011.63 Published online by Cambridge University Press

the coordination numbers determined by the occupancies of the Cu, In, and Se atoms in the Paszkowicz model closely agree with those determined by the XAFS analysis. The correspondence of the coordination numbers obtained by the analysis of the long-range order and the local structure indicates that the Paszkowicz model is a reliable candidate structure for $CuIn_3Se_5$.

Zhang et al.[24,25] and Maeda and Wada[26] showed that the defect pairs such as $(2V_{Cu} + In_{Cu})$ have particularly low formation energies for Cu-poor Cu–In–Se compounds. In the Paszkowicz model, the defect pairs of $(2V_{Cu} + In_{Cu})$ are formed with decreasing Cu/In ratio. In addition, V_{In} and Cu_{In} (substitution of Cu for In site) defects are also formed in the Paszkowicz model. Although this calculation revealed that the formation energies of V_{In} and Cu_{In} are higher than those of V_{Cu} and In_{Cu}, it is possible that the formation energy of a complex defect such as $(3V_{Cu} + V_{In} + 2In_{Cu} + Cu_{In})$ is lower than that of the defect pair of $(2V_{Cu} + In_{Cu})$ in Cu-poor Cu–In–Se compounds. It is difficult to calculate the formation energy of a complex defect because of the computational demands associated with the need to use a large supercell. The Paszkowicz model, at least, does not contradict the calculation results.

In the Se K-edge EXAFS analysis, the coordination number of the Se–Cu shell was found to decrease while that of the Se–In bond increased with decreasing Cu/In ratio from $CuIn_3Se_5$ to $CuIn_5Se_8$. However, the coordination numbers of Cu1–Se and Cu2–Se, obtained by a Cu K-edge EXAFS analysis, and those of In1–Se and the In2–Se, obtained by a In K-edge EXAFS analysis, exhibited negligible change with decreasing Cu/In ratio. These results clearly showed that the molar ratios of Cu1/Cu2 and In1/In2 do not change and that only the Cu (sum of Cu1 and Cu2)/In (sum of In1 and In2) ratio changes with decreasing Cu/In ratio. Using the molar ratio of Cu, In, and Se atoms in $CuIn_5Se_8$, we can estimate reasonable occupancy values for Cu1, Cu2, In1, and In2 (17%, 17%, 78%, and 93%, respectively) in the Pazkowicz model in Fig. 13(c).

V. CONCLUSION

We recorded XAFS spectra of a series of Cu_2Se–In_2Se_3 pseudobinary compounds and analyzed them in detail to elucidate the underlying crystal structure. An analysis of the Cu K-edge XANES and EXAFS spectra showed that the local structure about the Cu atom in the $CuInSe_2$, $Cu_{0.9}InSe_{1.95}$, $Cu_{0.82}InSe_{1.91}$, and $Cu_2In_3Se_{5.5}$ samples had a $CuSe_4$ tetrahedral character with the same Cu–Se bond length in spite of differing Cu/In ratios. However, a further decrease in the Cu/In ratio led to a change in the local structure about the Cu atom, and the $CuSe_4$ polyhedron was found to have two types of Cu–Se bonds in the $CuIn_3Se_5$ and $CuIn_5Se_8$ samples. Similar results for the local structure about the In atom were obtained from an analysis of the In K-edge XANES and EXAFS spectra, while the $CuIn_3Se_5$ and $CuIn_5Se_8$ samples exhibited an $InSe_4$ tetrahedral structure with differing In–Se bond lengths. From the results of a Se K-edge XANES analysis, it was expected that the coordination number of the Se–M (M = Cu or In) shell would decrease gradually with decreasing Cu/In ratio. A curve fitting analysis of the Se K-edge EXAFS showed that the coordination number of the Se–Cu shell decreased with decrease in Cu/In ratio. Moreover, the coordination number of the Se–In shell increased with decreasing Cu/In ratio over the range of $1/5 < Cu/In < 2/3$. From these XAFS results, we can determine the structure of the Cu-poor Cu–In–Se compounds. In the range $0.82 < Cu/In < 1$, the Cu-poor α phase assumes a chalcopyrite structure characterized by V_{Cu}. This is because only the coordination number of the Se–Cu in the local structure of the Se atom decreased with decreasing Cu/In ratio, while the other structural parameters resembled those in the $CuInSe_2$, $Cu_{0.9}InSe_{1.95}$, and $Cu_{0.82}InSe_{1.91}$ samples. For the case of the β phase compounds, $CuIn_3Se_5$ and $CuIn_5Se_8$, we compared the results obtained by an XAFS analysis with three postulated models. We conclude that a stannite-like structure with some cation (Cu and In) defects as shown in Fig. 13(c) can explain the XAFS results; in particular, the coordination numbers of all atoms have an influence. Since the model in Fig. 13(c) has the space group $I4(-)2m$ structure, this model does not contradict the structure determined from an electron diffraction analysis. Moreover, the structure of $CuIn_5Se_8$ can be estimated using the model shown in Fig. 13(c) and the analytical results of $CuIn_5Se_8$ obtained by XAFS. We conclude that the β phase structure of $CuIn_3Se_5$ and $CuIn_5Se_8$ is a stannite-like structure with some cation (Cu and In) defects as shown in Fig. 13(c).

ACKNOWLEDGMENTS

We thank Mr. Junya Kubo, Masaki Fukada, and Ms. Erika Tokumoto for their help in the XAFS measurement. We also thank Dr. Paul Fons of National Institute for Advanced Industrial Science & Technology for his critical reading of the manuscript. This work was in part supported by the Incorporated Administrative Agency New Energy and Industrial Technology Development Organization under the Ministry of Economy, Trade and Industry. This work was also supported in part by a grant from the High-Tech Research Center Program for private universities from the Japan Ministry of Education, Culture, Sports, Science and Technology.

REFERENCES

1. J.L. Shay, B. Tell, H.M. Kasper, and L.M. Schiavone: Electronic structure of $AgInSe_2$ and $CuInSe_2$. *Phys. Rev. B* **7**, 4485 (1973).

https://doi.org/10.1557/jmr.2011.63 Published online by Cambridge University Press

2. R. Herberholz, V. Nadenau, U. Rühle, C. Köble, H.W. Schock, and B. Dimmler: Prospects of wide-gap chalcopyrites for thin film photovoltaic modules. *Sol. Energy Mater. Sol. Cells* **49**, 227 (1997).
3. W. Höring, H. Neumann, H. Sobotta, B. Schumann, and G. Kühn: The optical properties of $CuInSe_2$ thin films. *Thin Solid Films* **48**, 67 (1978).
4. H.A. Weakleim and D. Redfield: Temperature dependence of the optical properties of silicon. *J. Appl. Phys.* **50**, 1491 (1979).
5. J.E. Jaffe and A. Zunger: Theory of the band-gap anomaly in ABC_2 chalcopyrite semiconductors. *Phys. Rev. B* **29**, 1882 (1984).
6. I. Repins, M.A. Contreras, B. Egaas, C. DeHart, J. Scharf, C.L. Perkins, B. To, and R. Noufi: 19.9%-efficient ZnO/CdS/$CuInGaSe_2$ solar cell with 81.2% fill factor. *Prog. Photovolt. Res. Appl.* **16**, 235 (2008).
7. M.A. Green, K. Emery, Y. Hshikawa, and W. Warta: Solar cell efficiency tables (version 53). *Prog. Photovoltaics Res. Appl.* **18**, 144 (2010).
8. D. Schmid, M. Ruckh, F. Grunwald, and H.W. Schock: Chalcopyrite/defect chalcopyrite heterojunctions on the basis of $CuInSe_2$. *J. Appl. Phys.* **73**, 2902 (1993).
9. L.S. Palatnik and E.J. Rogacheva: Phase diagrams and structure of some semiconductor $A_2^{I}C^{VI}$-$B_2^{III}C^{VI}$ alloys. *Sov. Phys. Dokl.* **12**, 503 (1967).
10. W. Hönle, G. Kühn, and U.C. Boehnke: Crystal structures of two quenched Cu-In-Se phases. *Cryst. Res. Technol.* **23**, 1347 (1988).
11. B.H. Tseng and C.A. Wert: Defect-ordered phases in a multiphase Cu-In-Se material. *J. Appl. Phys.* **65**, 2254 (1989).
12. K.S. Knight: The crystal structures of $CuInSe_2$ and $CuInTe_2$. *Mater. Res. Bull.* **27**, 161 (1992).
13. H.Z. Xiao, L.C. Yang, and A. Rockett: Structural, optical, and electrical properties of epitaxial chalcopyrite $CuIn_3Se_5$ films. *J. Appl. Phys.* **76**, 1503 (1994).
14. S. Nomura and S. Endo: Preparation and structural analysis of ordered vacancy compounds in the Cu-In-Se system. *MRS Jpn.* **20**, 755 (1996).
15. T. Hanada, A. Yamana, Y. Nakamura, O. Nittono, and T. Wada: Crystal structure of $CuIn_3Se_5$ semiconductor studied using electron and X-ray diffractions. *Jpn. J. Appl. Phys.* **36**, L1494 (1997).
16. J.M. Merino, S. Mahanty, M. Leon, R. Diaz, F. Rueda, and J.L.M.d. Vidales: Structural characterization of $CuIn_2Se_{3.5}$, $CuIn_3Se_5$ and $CuIn_5Se_8$. *Thin Solid Films* **361/362**, 70 (2000).
17. C.H. Chang, S.H. Wei, J.W. Johnson, S.B. Zhang, N. Leyarovska, G. Bunker, and T.J. Anderson: Local structure of $CuIn_3Se_5$: X-ray absorption fine structure study and first-principles calculations. *Phys. Rev. B* **68**, 054108 (2003).
18. W. Paszkowicz, R. Lewandowska, and R. Bacewicz: Rietveld refinement for $CuInSe_2$ and $CuIn_3Se_5$. *J. Alloy. Comp.* **362**, 241 (2004).
19. U.C. Boehnke and G. Kühn: Phase relations in the ternary system Cu-In-Se. *J. Mater. Sci.* **22**, 1635 (1987).
20. B. Tell, J.L. Shay, and H.M. Kasper: Room-temperature electrical properties of Te I-III-VI_2 semiconductors. *J. Appl. Phys.* **43**, 2469 (1972).
21. J. Parkes, R.D. Thomlinson, and M.J. Hampshiere: Electrical properties of $CuInSe_2$ single crystals. *Solid State Electron.* **16**, 773 (1973).
22. P. Migliorato, J.L. Shay, H.M. Kasper, and S. Wagner: Analysis of the electrical and luminescent properties of $CuInSe_2$. *J. Appl. Phys.* **46**, 1777 (1975).
23. R. Noufi, R. Axton, C. Herrington, and S.K. Deb: Electronic properties versus composition of thin films of $CuInSe_2$. *Appl. Phys. Lett.* **45**, 668 (1984).
24. S.B. Zhang, S.H. Wei, and A. Zunger: Stabilization of ternary compounds via ordered arrays of defect pairs. *Phys. Rev. Lett.* **78**, 4059 (1997).
25. S.B. Zhang, S.H. Wei, and A. Zunger: Defect physics of the $CuInSe_2$ chalcopyrite semiconductor. *Phys. Rev. B* **57**, 9642 (1998).
26. T. Maeda and T. Wada: Characteristics of chemical bond and vacancy formation in chalcopyrite-type $CuInSe_2$ and related compounds. *Phys. Status Solidi C* **6**, 1312 (2009).
27. N. Kohara, S. Nishiawaki, T. Negami, and T. Wada: Physical vapor deposition of hexagonal and tetragonal $CuIn_5Se_8$ thin films. *Jpn. J. Appl. Phys.* **39**, 6316 (2000).
28. R. Bacewicz, A. Wolska, K. Lawniczak-Jablonska, and P. Sainctavit: X-ray absorption near-edge structure of $CuInSe_2$ crystals. *J. Phys. Condens. Matter* **12**, 7371 (2000).
29. A. Wolska, R. Bacewicz, J. Fillipowicz, and K. Attenkofer: X-ray absorption near-edge structure of selenium in the Cu-In-Se system. *J. Phys. Condens. Matter* **13**, 4457 (2001).
30. J.M. Merino, S. Díaz-Moreno, G. Subías, and M. Leön: A comparative study of Cu-Se and In-Se bond length distributions in $CuInSe_2$ with related In-rich compounds. *Thin Solid Films* **480/481**, 295 (2005).
31. R. Lewandowska, R. Bacewicz, and J. Fillipowicz: EXAFS study of In-rich phases in Cu-In-Se system. *Cryst. Res. Technol.* **37**, 235 (2002).
32. T. Wada, H. Kinoshita, and S. Kawata: Preparation of chalcopyrite-type $CuInSe_2$ by non-heating process. *Thin Solid Films* **431/432**, 11 (2003).
33. A.L. Ankudinov, B. Ravel, J.J. Rehr, and S.D. Conradson: Real-space multiple-scattering calculation and interpretation of x-ray-absorption near-edge structure. *Phys. Rev. B* **58**, 7565 (1998).
34. N. Kosugi, Y. Tokura, H. Takagi, and S. Uchida: Cu K-edge x-ray absorption near-edge structure and electronic structure of $Nd_{2-x}Ce_xCuO_{4-y}$ and $La_{2-x}Sr_xCuO_4$. *Phys. Rev. B* **41**, 131 (1990).
35. T. Yamamoto, T. Tanaka, S. Suzuki, R. Kuma, K. Teramura, Y. Kou, T. Funabiki, and S. Yoshida: NO reduction with CO in the presence of O_2 over Cu/Al_2O_3 (3)—Structural analysis of active species by means of XAFS and UV/VIS/NIR spectroscopy. *Top. Catal.* **18**, 113 (2002).
36. M. Sano, S. Komorita, and H. Yamatera: XANES spectra of copper (II) complexes: Correlation of the intensity of the $1s \rightarrow 3d$ transition and the shape of the complexes. *Inorg. Chem.* **31**, 459 (1992).
37. H.W. Spiess, U. Haeberln, G. Brandt, A. Räuber, and J. Schneider: Nuclear magnetic resonance in I_B-III-VI_2 semiconductors. *Phys. Status Solidi B* **62**, 183 (1974).
38. G. Zahn and P. Paufler: Identification of predominant point defects in nonstoichiometric $CuInSe_2$ by x-ray powder diffraction. *Cryst. Res. Technol.* **23**, 499 (1988).
39. J.M. Merino, J.L. Martin de Vidales, S. Mahanty, R. Diaz, F. Rueda, and M. León: Composition effects on the crystal structure of $CuInSe_2$. *J. Appl. Phys.* **80**, 5610 (1996).
40. F. Frolow, L. Chernyak, D. Cahen, H. Hallak, J. Gabboun, A. Kvick, and H. Graafama: Ternary and multinary compounds. *Inst. Phys. Conf. Ser.* **152**, 67 (1998).
41. J. T-Thienprasert, J. Nukeaw, A. Sungthong, S. Porntheeraphat, S. Singkarat, D. Onkaw, S. Rujirawat, and S. Limpijumnong: Local structure of indium oxynitride from x-ray absorption spectroscopy. *Appl. Phys. Lett.* **93**, 051903 (2008).
42. L. Gastaldi, M.G. Simeone, and S. Viticoli: Structure refinement of $ZnIn_2Se_4$. *J. Solid State Chem.* **66**, 251 (1987).
43. R.E. March and W.R. Robinson: On the structure of $ZnIn_2Se_4$. *J. Solid State Chem.* **73**, 591 (1988).

https://doi.org/10.1557/jmr.2011.63 Published online by Cambridge University Press